IFSCC 2025 full paper (IFSCC2025-858)

"Photoacoustic-ultrasound dual-mode microscopic imaging of depth-resolved melanin distribution in facial skin for assessment of aging"

Jian Mu [1], Simin Lin [1], Xiao Feng [1], Yuying Wang [1], Yun Wei [1], Jing Wang [1]*, and Hu Huang [1]

[1] PROYA COSMETICS CO.,LTD, China

1. Introduction

Melanin is a dominant chromophore related to light absorption in skin including ultraviolet (UV), visible, and near-infrared spectral regions [1, 2]. Melanin content and its depth distribution play key roles in determining visualized skin color [3, 4]. Epidermal melanin is synthesized and stored in melanosomes[5], which is produced by melanoctes locating in the basal layers of the epidermis, and contains multiple pigments including brown or black eumelanin and red or yellow pheomelanin [6].

In dermatology, melanometers use visible and near-infrared reflectance measurement to measure skin color [7], which use the International Commission on Illumination (CIE) L*a*b* color space for quantitative skin color classification [8]. The first quantative evaluation of skin color was performed in 1939 by Edwards and Duntley[9]. And individual typology angle (ITA) [7] has been used as objective parameter to classify the skin color. However, it has been criticized for being subjective and susceptible to inter-operator variability[10, 11], since this method do not measure actual melanin content. Thus, there is growing support to address the need for improved methods to quantify melanin content.

There are several optical methods developed to detect melanin in biological tissues, which can roughly be categorized into invasive imaging and noninvasive imaging methods. The invasive imaging includes the histological cuts with various staining [12], scanning electron microscopy [13], and femtosecond time-resolved pump-probe microscopy for excised tissue [14]. However, the primary disadvantage of reference techniques is that they are destructive and require invasive skin biospy.

And noninvasive imaging methods contains confocal microscopy[15], multi-photon imaging[15-17], multiphoton FLIM[18], and raman microspectroscopy [19]. Nonetheless, the penetration depth of these imaging technique is sufficient for capturing the entire thickness of the epidermis on most areas of the body. Another noninvasive imaging techniques also includes diffused reflectance spectroscopy [20, 21], spatial frequency domain imaging (SFDI) [22, 23], and polarization-sensitive optical coherence tomography[24-26] for quantifying melanin content. However, these techniques cannot provide the informaion of the depth-resolved melanin distribution.

Photoacoustic (PA) microscopy (PAM) offers a non-invasive, sensitive, and quantitative tool for melanin characterization [27, 28] and melasma [29] based on the absorption of melanin. The light source of 650 nm was applied to measure the melanin, and it was shown that the volume of melanin structure increases with aging [30]. However, the depth-resolved distribution of melanin was not insufficient. In this study, high-frequency ultrasound image-guide PAM was employed for depth-resolved distribution of melanin in skin. The deep learning was used to locate the boundary of irregular skin. Then the relationship between skin pigmentation, age and depth-resolved melanin was analyzed.

2. Materials and Methods

2.1 Subjects

This work was performed in compliance with the ethical rules for human experimentation and approved by the Fujian Normal University. 46 volunters were recruited for this study, where 26 individuals in the 20-29 age group and 20 individuals in the 50-59 age group. Subjects signed an informed written consent prior to participation. All subjects were scanned over cheek. An area measuring approximately 6mm×6mm was scanned. Before the human skin was imaged, the volunteers were required to remove makeup anrequired to decode how depth-specific melanin distribution modulates skin color heterogeneity.

In this study, the high-frequency ultrasound clean the entire face to rule out the influence of cosmetics on the imaging results. Measurement of skin pigmentation at cheek region was obtained using colorimeter (Konica Minolta, CM-700d) that provided values in CIE L*a*b color space, which provided quantitative point measurements of skin color.

2.2 Photoacoustic-ultrasound dual-mode microscopy

Photoacoustic-ultrasound dual-mode microscopy (HadatomoZ WEL 5200, Advantest, Tokyo, Japan) was applied in this study. The system is capable of dual-wavelength PA and ultrasoud imaging. The center frequency of the ultrasound snesor is 60 MH, enabling high resolution in-vivo imaging. The dual-wavelength light sources were 575 nm and 650 nm. The pulse energy is less than 18 uJ at 575 nm and less than 14 uJ at 650nm. The repetition rate is 1000Hz and the pulse width is less than 10ns for each [30]. The measurement region was 6 mm×6 mm with a 30 um scanning step along the vertical direction of the skin.

Figure 1 shows that the boundary of skin and coupling film can be seen clearly in the cross-section ultrasound image for cheek skin. Figure 1 (b) shows x-z spatial distribution of melanin, since 650 nm represents melanin absorption. Figure 1 (d) indicates the blood distribution, because that the clear blood vessel image can be obtained by subtracting 650 nm PA from 575 nm PA signals [31].

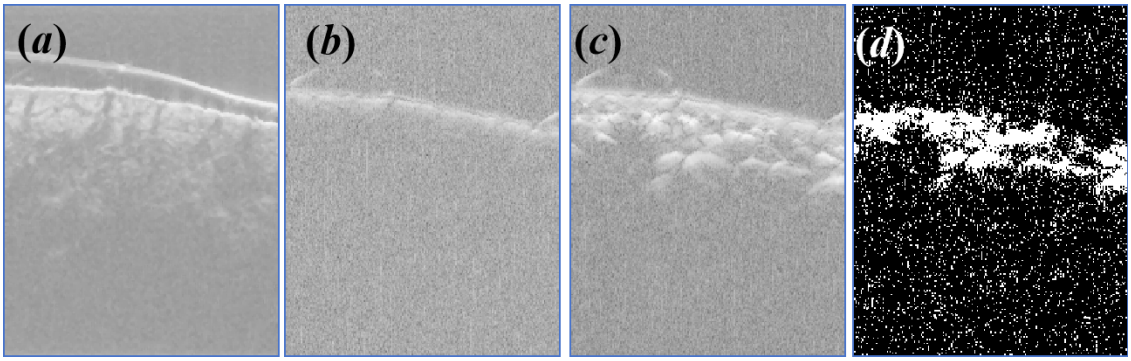

Figure 1. Cross-sectional of (a) ultrasound image, (b) PA image at the wavelength of 650 nm, (c) PA image at the wavelength of 575 nm and (d) the difference of PA image at 575 nm and 650 nm for cheek skin. Image size = 3.84 mm×6 mm.

2.3 PA intensity depending on melanin in skin

PA produces signal as a function of the absorption coefficient μ_a [32], and the intensity I of PA signal is directly proportional to μ_a, which can be expressed as $I = \mu_a \cdot \Gamma \cdot \Phi$[33], where Γ is the Grüneisen parameter, Φ is the local fluence. Eumelanin and pheomelanin exhibit similar absorption spectra, and are often considered as a single chromophore in VIS-NIR studies[34]. The spatial resolved epidermal tissue absorption can be calculated as follows[2, 35]:

$$\mu_{a,epi}(\lambda) = \left(M_f \cdot \mu_{a,mel}(\lambda) + \left(1 - M_f\right) \cdot \mu_{a,0}(\lambda)\right)(1 - C_{wat}) + C_{wat} \cdot \mu_{a,wat}(\lambda)$$

where M_f is the mean volume fraction of melanin in the epidermis, $\mu_{a,mel}$ is the absorption coefficient of a typical melanin, $\mu_{a,0}$ is the "baseline" absorption coefficient of epidermal tissue without melanin, C_{wat} is concentration of water, $\mu_{a,wat}$ is the absorption coefficient of water and λ is wavelength in nm. The following equations can be used to determin $\mu_{a,mel}$ [36] and $\mu_{a,0}$ [35]:

$$\mu_{a,mel} = (519cm^{-1})\left(\frac{\lambda}{500nm}\right)^{-3.53} \quad and \quad \mu_{a,0} = 7.84 \times 10^7 \lambda^{-3.255}.$$

Thus, the spatial resolved PA intensity is proportional to local volume fraction of melanin.

2.4 Segmentation of skin boundary in ultrasound image based on deep learning

In order to accurate the depth-resolved distribution of melanin, irregular skin surfaces must be localized and planarized. Firstly, the irregular skin boundary imaged by cross-sectional high-frequency ultrasound image can be located based on convolutional neural network (CNN) employing U-net architecture, which can be a good solution for the adaptive and automatic segmentation of medical images [37]. The methos is similar to our previous work [38]. After segmentation [Fig.2 (a)], the boundary of skin can be recorded in Fig.2 (b). Meanwhile, the skin boundaries observed in melanin [Fig.2 (c)] and vessel imaging [Fig.2 (d)] align precisely with those detected in ultrasound images. Then, align the irregular skin boundaries to a uniform height, transforming uneven edges into a flat surface, and the horizontal section images (X-Y plane) including melanin map and blood vessels image can be reconstructed, which is important basis to quantitiatively characterize the depth-resolved distribution of melanin. Finally, all images can be combined to form a multi-modal fused 3D image shown in Fig.2 (e), in which the skin structure, melanin and blood vessel can be seen clearly.

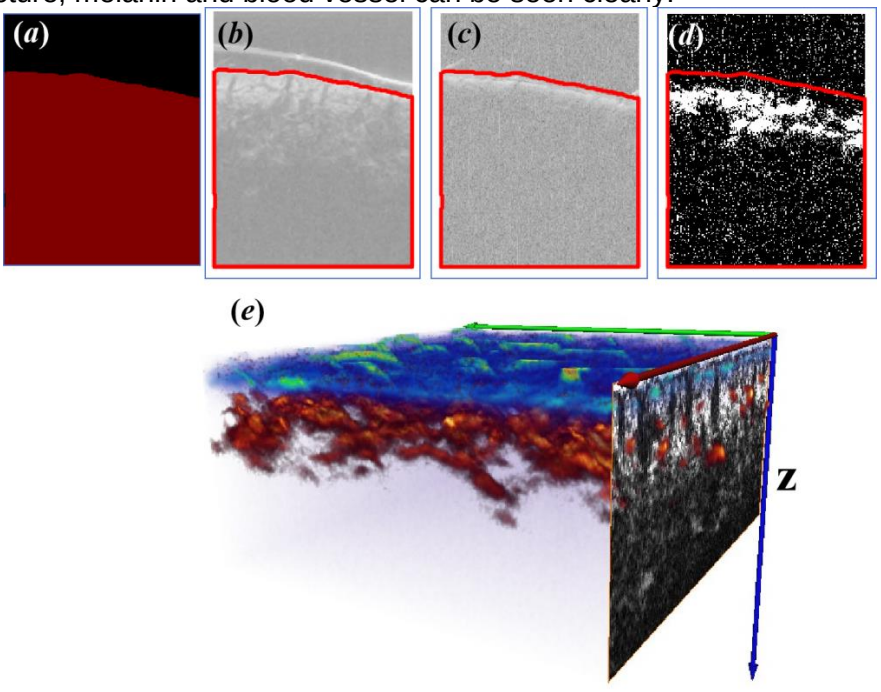

Figure 2. (a) Segmentation of ultrasound image of skinbased on CNN in Figure 1 (a), (b) the boundary of ultrasound image in Figure 1 (a), (c) the boundary in melanin image in Figure 1 (b), (d) the boundary

in blood vessel image in Figure 1 (d), and (e) the multi-modal fused 3D image, in which cross-sectional gray image denotes ultrasound image for skin structure, dark blue image is 3D melanin, and dark red image is blood vessel.

2.5 Statistics

The error bars in all plots represents standard deviation. All significance testing was done using two independent samples t-test, whose core algorithm depends on the unequal variances of the two samples p-value < 0.05 was considered significant.

3. Results

3.1 Depth-dependent spatial distribution of melanin

Figure 3 (a)-(d) show the en-face spatial distribution of melanin at the different depths of cheek skin based on PA image at the wavelength of 650 nm, and Figure 3(e) indicates the three-dimensional spatial distribution of melanin. Melanin is produced by melanocytes residing in the basal layer of the epidermis, which is the deepest layer of the epidermi and immediately adjacent to the DEJ, whose undulations with its ridges and papillae. Figure 3(c) demonstrates the en-face melanin distributed surrounding the DEJ, whose morphogy is similar to that imaged by miltiphoton microscopy[18, 39]. In addition, Figure 3 (f) demonstrates the depth-dependent PA intensity, which can be divided into three regions including keratinized layer, basal layer and superficial dermis based on PA intensity.

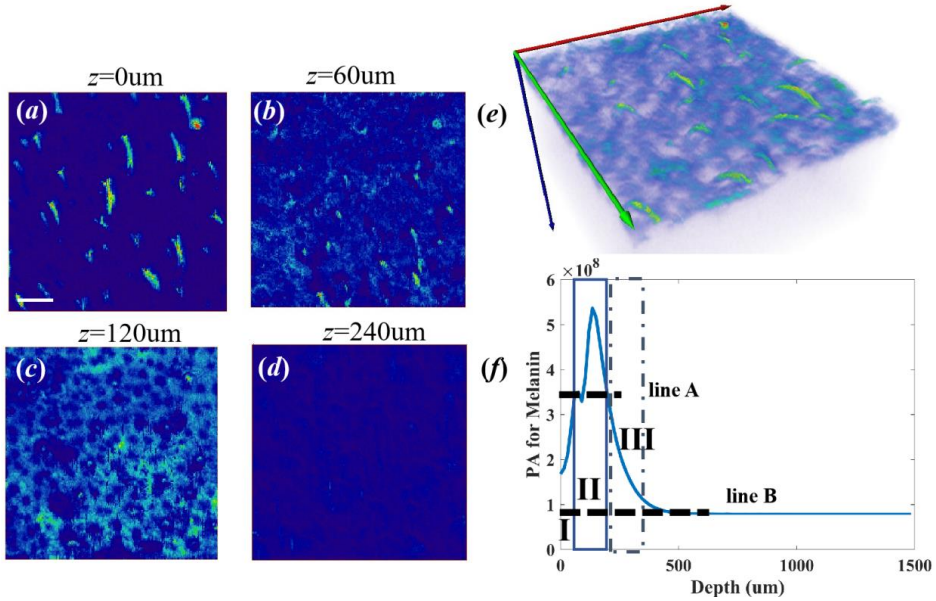

Figure 3. Depth-dependent spatial distribution of melanin in cheek skin based on PA image at the wavelegth of 650 nm, (a) z=0 μm, (b) z=60 μm, (c)z=120 μm, (d)z=240 μm, and (e) 3D melanin image. Image size =6 mm×6 mm, scalebar is 1 mm. (f) depth-dependent PA intensity. Line A indicates half of the dfference between the maximum and minimum values, and line B is the ground PA intensity due to “baseline” absorption of epidermal tissue without melanin. Depth-dependent curve can be divided into three regions including keratinized layer(I), basal layer (II) and superficial dermis (III).

3.2 ITA-dependent melanin

In order to study the relationship between skin pigmentation and melanin, their pigmentary phenotypes of cheek skin were assessed with a colorimeter and classified according to their ITA. ITA values that are linearly correlated to the melanin content [Figure 4(a)] allowed us to define three groups that include [20-30] (n = 7), [30-40] (n = 20), and [40-50] (n =13). Figure 4 (b) represent over 70% of the total melanin of the epidermis in the basal layer. In addition, the larger ITA values, the greater the proportion of melanin. These observations are consistent

with previous studies [40], since they mainly reported the distribution of melanosomes in the basal layer.

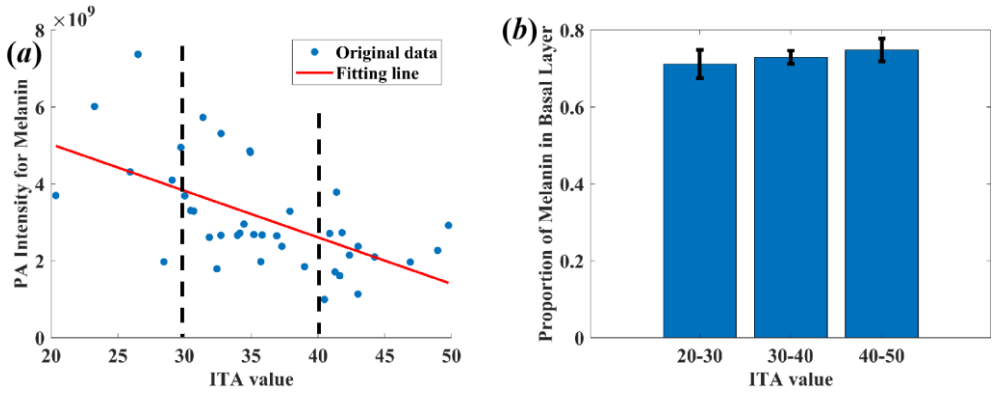

Figure 4. (a) Significant correlation between the summation of PA intensity of melanin content and ITA. Based on ITA values, skin sampels were divided into three groups: 20-30, 30-40, 40-50, (b) the proportion of Melanin in basal layer of cheek skin versus ITA value.

3.3 Age-related melanin

In order to age-dependent characterization of melanin, the typica melaninl measurement results for the young (20+s) and old (50+s) in divaiduals are shown in Figure 5 (a) and (g), respectively, at the approximately equal ITA values. The PA signal was less apparent in the younger group. Contrarily, the PA signal was clearly visible in the older group. Meanwhile, in older individuals, melanin tends to exist at greater depths within the cheek skin by comparing the melanin map in the different depth in Figure 5. Additionally, a torus-like pattern structure was observed as indicated by the arrows in the figure, which tended to increase with age.

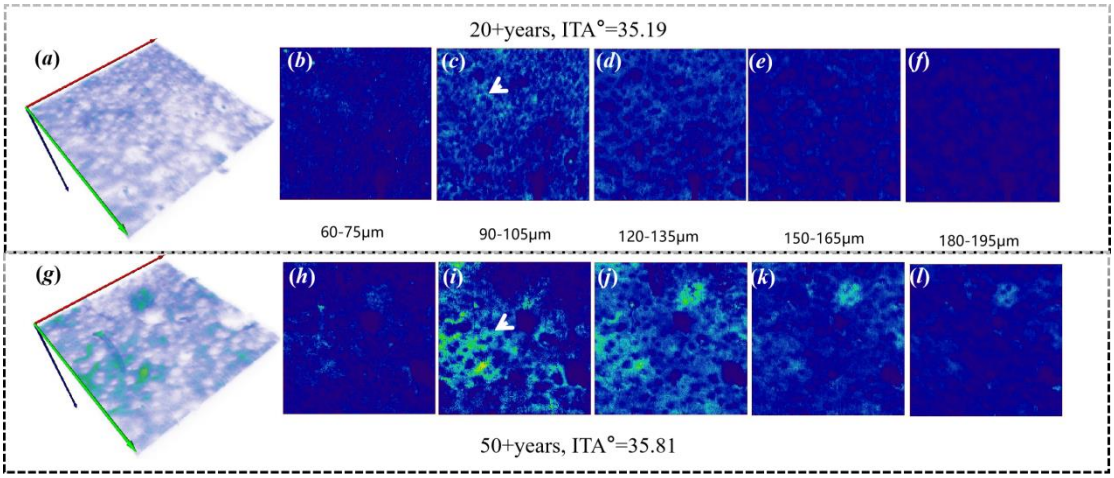

Figure 5. The typical difference of melanin distribution between young (20+years) and old (50+years) at the approximately equal ITA values (ITA~35). (a) and (g) are three-dimensional melanin distribution, others are en-face spatial distributions of melanin at the different depths. The white arrows are torus-like pattern structures.

Figure 6 (a) shows significantly higher average ITA values in 20-29-year-olds compared to those in 50-59 year-olds. However, ITA is a superficial colorimetric index, not a definitive tool for evaluating internal melanin distribution. Figures 6 (b)-(d) demonstrate that PA intensity increase with age at the keratinized layer, basal layer and superficial dermis, respectively. PA intensity of melanin deposition in the basal layer shows marked contrasts between young and aged skin in Figure 6 (b). However, there is no obviously difference of PA intensity in the keratinized layer and superficial dermis between young and aged skin in Figures 6 (c) and (d). This is because melanin in the keratinized layer, especially the stratum corneum, is shed

rapidly, unlike melanin in basal layer that accumulates with aging. In addition, the increase in melanin in the keratinized layer of young and elderly skin is similar after the same amount of sun exposure, masking the age difference.

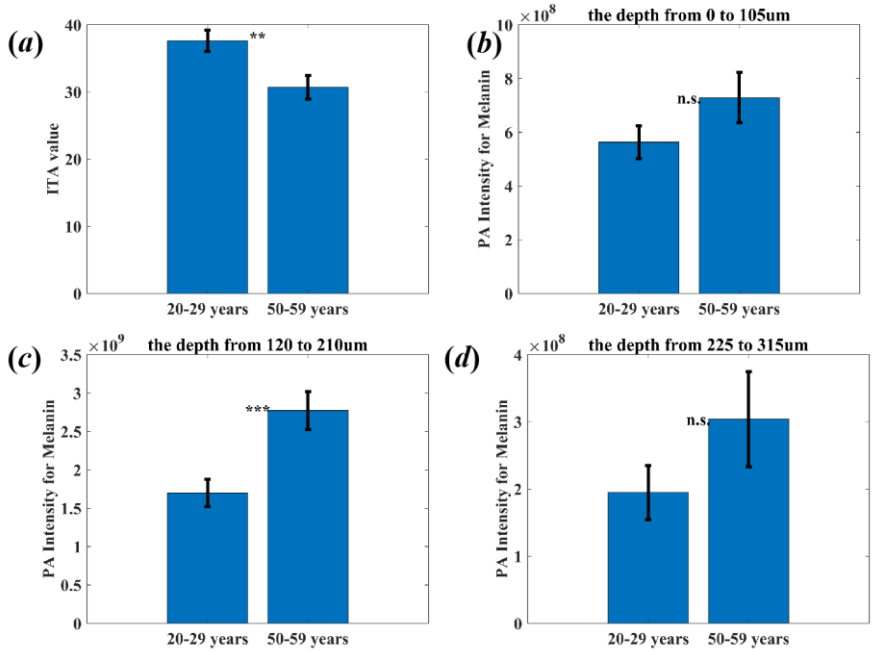

Figure 6. (a) ITA difference and PA intensity in (b) the keratinized layer, (c) basal layer and (d) superficial dermis between young (20+years) and old (50+years). '***','**', '*'and 'n.s.' denote $p < 0.001$, $p < 0.01$, $p < 0.05$, and $p \geq 0.05$, respectively.

To reflects the relationship between internal melanin deposition and surface colorimetric characteristics, the ratio γ_{ita} of total melanin content to ITA value was proposed. Figure 7 indicates that the ratio of PA intensity for melanin to ITA value in dffierent depths of young cheek skin is lower than that of elder group, and there are clear distinctions in the ratio in the keratinized layer and the basal layer of skin between young and elder groups.Addionally, the ratio in the keratinized layer of elderly skin is approximately 1.71 times that of young group, and the ratio in the basal layer of elderly skin is about 1.99 times that of young group. The reasons are that balanced melanin synthesis and clearance, and intact epidermal barrier confines melanin to superficial layers for young skin. However, there is no obvious distinction between young and elder groups in superficial dermis shown in Figure 7 (c), although the mean of PA intensty in elder group is higher than the young group, because not every melanin in aged skin reaches the dermis.

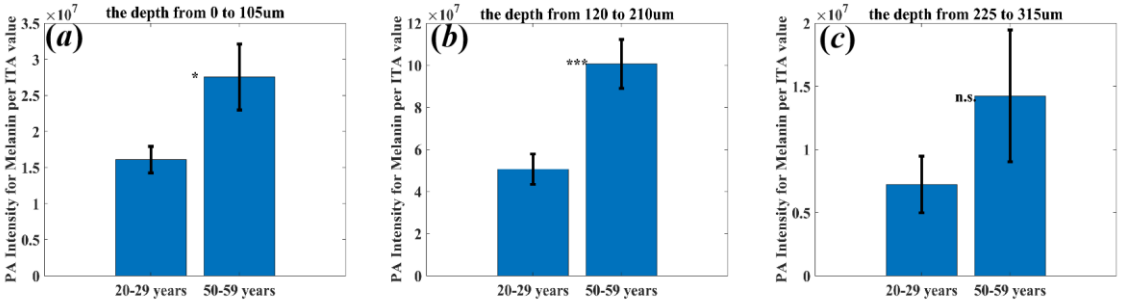

Figure 7. The ratio γ_{ita} of PA intensity for melanin to ITA value at the different depths (a)the keratinized layer, (b) basal layer and (c) superficial dermis between young (20+years) and old (50+years). '***','**', '*'and 'n.s.' denote $p < 0.001$, $p < 0.01$, $p < 0.05$, and $p \geq 0.05$, respectively.

To reveal the dynamic relationship between melanin accumulation and age, the ratio γ_{age} of PA intensity of melanin content to age seen as annual melanin deposition was presented for quantifying skin feature. Figure 8 (a) demonstrates that the ratio γ_{age} in the keratinized layer of young skin is higher than that of elder group, and there is obvious diffference. Although lower total melanin content in young group [Figure 6 (b)], the annual melanin deposition is higher than that of elder group. Furthermore, there is no obvious difference of annual melanin deposition in the basal layer and the superficial dermis between young group and elder group in Figures 8 (b) and (c), although the higher total melanin content in elder group. This is because annual melanin deposition approximatelly equal due to photoaging and natural aging, which results in the accumation of melainin.

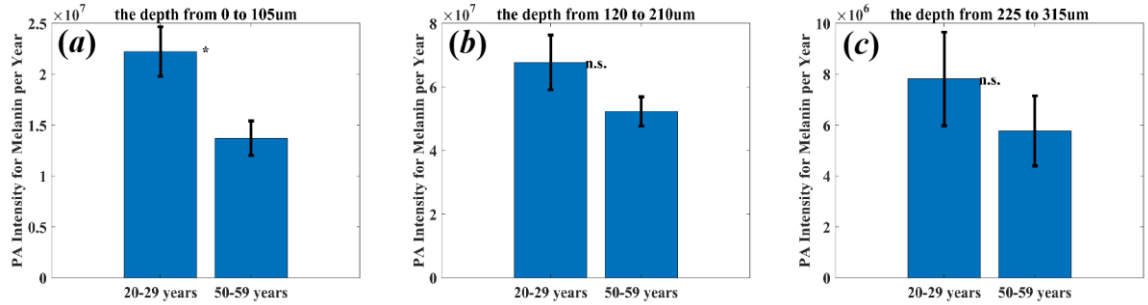

Figure 8. The ratio γ_{age} of PA intensity for melanin to ITA value at the different depths (a)the keratinized layer, (b) basal layer and (c) superficial dermis between young (20+years) and old (50+years). '***','**', '*'and 'n.s.' denote p < 0. 001, p < 0.01, p < 0.05, and p ≥ 0.05, respectively.

4. Discussion

In this study, high-frequency ultrasound image-guide photoacoustic microscopy was proposed for depth-resolved distribution of melaninin skin. In this method, PA intensity directly measure the melanin density based on absorption coefficient of melanin, which is linearly related to the volume fraction of melanin. And the difference of spatial distribution of melanin in the various depth of skin can be seen clearly, and it provided a non-invasive mehtod to estimate the proportion of the total melanin of the epidermis in the basal layer. In addition, another advantage is that the image depth for melanin can reach the dermal layer of skin, which could be used to melasma subtyping (epidermal and dermal subtypes)[29], since they require different therapies [41].

The ratio γ_{ita} of total melanin content to ITA value and the ratio γ_{age} of PA intensity of melanin content to age were employed for characterization of cheek skin. The ratio γ_{ita} indicates melanin content per unit of surface color typology, and the ratio γ_{ita} in in the keratinized layer and the basal layer of skin of young cheek skin is lower than that of elder group, which means that older individuals require metabolizing more melanin content than younger ones for changing per ITA value. Thus, the ratio γ_{ita} could be a potential parameter for skin whitening.

However, the ratio γ_{age} in the keratinized layer of young skin is higher than that of elder group, which mean that the younger skin requires timely management to prevent excessive accumulation. And there is no obvious difference of the ratio γ_{age} between yong and elder group in the basal layer, which implies that a dynamic equilibrium is stable in healthy skin between melanin synthesis and clearance during aging, and anti-aging care should be prioritized across all age groups. Thus, the ratio γ_{age} can be used as an indicator for anti-aging of skin.

The limitation of this method is that PA microscopy cannot see directly melanosomes, in which melanin is produced in the basal layer of the epidermis, since the spatial resolution used in this

study is approximately 30um. Furthermore, PA imaging has difficulty differentiating subtypes of melanin,which can be classified in brown-black eumelanin and yellow-red pheomelanin, because they share similar linear absorption properties. And the multispectral PAM is expected to be applied to melanin classification, since dependence on wavelength of the melanin absorption spectrum [20].

5. Conclusion

Accurate depth-resolved melanin content measurement based on high-frequency ultrasound image-guide photoacoustic microscopy provides a high quality metric for skin by combining with deep learning for locating the irregular boundary of skin. The results indicated the over 70% of the total melanin of the epidermis in the basal layer. In addition, the ratio γ_{ita} of total melanin content to ITA value and the ratio γ_{age} of PA intensity of melanin content to age in the keratinized layer and the basal layer of skin have obvious features between young and elder group, which suggests that these two parameters could be potential applications for evaluating whitening and anti-aging of skin, respectively. Thus, this method should drive advancements in dermatological therapies, anti-aging strategies, and cosmetic innovation.

References

1. Handbook of Cosmetic Science and Technology. 5th Edition ed. 2022, Boca Raton: CRC Press.
2. Jacques, S.L., Quick analysis of optical spectra to quantify epidermal melanin and papillary dermal blood content of skin. Journal of Biophotonics, 2015. 8(4): p. 309-316.
3. Kristian P. Nielsen, L.Z., Jakob J. Stamnes, Knut Stamnes, Johan Moan, The importance of the depth distribution of melanin in skin for DNA protection and other photobiological processes. Journal of Photochemistry and Photobiology B: Biology, 2006. 82(3): p. 194-198.
4. H-Y Thong, S.-H.J., C-C Sun, R E Boissy, The patterns of melanosome distribution in keratinocytes of human skin as one determining factor of skin colour. British Journal of Dermatology, 2003. 149(3): p. 498-505.
5. Taketsugu Tadokoro, Y.Y., Jan Batzer, Sergio G. Coelho, Barbara Z. Zmudzka, Sharon A. Miller, Rainer Wolber, Janusz Z. Beer, Vincent J. Hearing, Mechanisms of Skin Tanning in Different Racial/Ethnic Groups in Response to Ultraviolet Radiation. Journal of Investigative Dermatology, 2005. 124(6): p. 1326-1332.
6. William J Pavan, R.A.S., The Genetics of Human Skin and Hair Pigmentation. Annual Review of Genomics and Human Genetics, 2019. 20: p. 41-72.
7. Sandhya Vasudevan, W.C.V., Sandy Weininger, T Joshua Pfefer, Melanometry for objective evaluation of skin pigmentation in pulse oximetry studies. Communications Medicine, 2024. 4: p. 138.
8. Lucio Andreassi, L.F., Practical applications of cutaneous colorimetry. Clinics in Dermatology, 1995. 13: p. 369-373.
9. Edward A. Edwards, S.Q.D., The pigments and color of living human skin. The American Journal of Anatomy, 1939. 65(1): p. 1-33.
10. Norton, H.L., Variation in pulse oximetry readings: melanin, not ethnicity, is the appropriate variable to use when investigating bias. Anaesthesia, 2022. 77(3): p. 354-355.
11. Olubunmi E Okunlola, M.S.L., Paul B Batchelder, Michael Bernstein, John R Feiner, and Philip E Bickler, Pulse Oximeter Performance, Racial Inequity, and the Work Ahead. Respiratory Care, 2022. 67(2): p. 252-257.
12. Nicolas Joly-Tonetti, J.W., M. Bell, DJ Tobin, Melanin fate in the human epidermis: a reassessment of how best to detect and analyse histologically. Experimental Dermatology, 2016. 25(7): p. 501-504.

13. Peter Gouras, K.B., Lena Ivert, Martha Neuringer, A novel melano-lysosome in the retinal epithelium of rhesus monkeys. Experimental Eye Research, 2011. 93(6): p. 937-946.
14. Bohan Zhang, T.Y., Yaxin Chen, Chuqiao Wang, Yongyang Bao,Zhaoyang Wang, Keke Zhao and Minbiao Ji, Label-Free Delineation of Human Uveal Melanoma Infiltration With Pump–Probe Microscopy. Frontiers in Oncology, 2022. 12: p. 891282.
15. Ali Majdzadeh, A.M.D.L., Hequn Wang, Harvey Lui, David I. McLean, Richard I. Crawford, David Zloty, Haishan Zeng, Real‐time visualization of melanin granules in normal human skin using combined multiphoton and reflectance confocal microscopy. Photodermatology, Photoimmunology & Photomedicine, 2015. 31(3): p. 141-148.
16. Rolf B. Saager, M.B., Viera Crosignani, Ata Sharif, Anthony J. Durkin, Kristen M. Kelly, and Bruce J. Tromberg, In vivo measurements of cutaneous melanin across spatial scales: using multiphoton microscopy and spatial frequency domain spectroscopy. Journal of Biomedical Optics, 2015. 20(6): p. 066005.
17. Juvinch R. Vicente, A.D., Kristina Shrestha & Mihaela Balu, In vivo imaging with a fast large-area multiphoton exoscope (FLAME) captures the melanin distribution heterogeneity in human skin. Scientific Reports, 2022. 12: p. 8106.
18. Ana‐Maria Pena, E.D., Sébastien Brizion, Peggy Sextius, Serge Koudoro, Thérèse Baldeweck, EmmanuelleTancrède‐Bohin, In vivo melanin 3D quantifcation and z‐epidermal distribution by multiphoton FLIM, phasor and Pseudo‐FLIM analyses. Scientifc Reports, 2022. 12: p. 1642.
19. B. P. Yakimov, E.A.S., J. Schleusener, A. S. Allenova, V. V. Fadeev & M. E. Darvin, Melanin distribution from the dermal–epidermal junction to the stratum corneum: non-invasive in vivo assessment by fluorescence and Raman microspectroscopy. Scientifc Reports, 2020. 10: p. 14374.
20. Renato Marchesini, A.B., Mauro Carrara, In vivo characterization of melanin in melanocytic lesions: spectroscopic study on 1671 pigmented skin lesions. Journal of Biomedical Optics, 2009. 14(1): p. 014027.
21. George Zonios, A.D., Mauro Carrara, Renato Marchesini, In vivo optical properties of melanocytic skin lesions: common nevi, dysplastic nevi and malignant melanoma. Photochemistry and Photobiology, 2010. 86(1): p. 236-240.
22. Thinh Phan, R.A.R., Adrien Ponticorvo, Binh C. Le, Seyed A. Sharif, Gordon T. Kennedy, Robert H. Wilson, Anthony J. Durkin, Quantifying the confounding effect of pigmentation on measured skin tissue optical properties: a comparison of colorimetry with spatial frequency domain imaging. Journal of Biomedical Optics, 2022. 27(3): p. 036002.
23. Thinh Phan, R.R., Adrien Ponticorvo, Binh C. Le, Robert H. Wilson, Seyed A. Sharif, Gordon T. Kennedy, Nicole P. Bernal, Anthony J. Durkin, Characterizing reduced scattering coefficient of normal human skin across different anatomic locations and Fitzpatrick skin types using spatial frequency domain imaging. Journal of Biomedical Optics, 2021. 26(2): p. 026001.
24. Yamanari, M., et al., Melanin concentration and depolarization metrics measurement by polarization-sensitive optical coherence tomography. Scientific Reports, 2020.
25. Bernhard Baumann, S.O.B., Thomas Konegger, Michael Pircher, Erich Götzinger, Ferdinand Schlanitz, Christopher Schütze, Harald Sattmann, Marco Litschauer, Ursula Schmidt-Erfurth, Christoph K Hitzenberger, Polarization sensitive optical coherence tomography of melanin provides intrinsic contrast based on depolarization. Biomedical Optics Express, 2012. 3(7): p. 1670-1683.
26. Norman Lippok, B.B., Martin Villiger, Wang-Yuhl Oh, Benjamin J. Vakoc, Brett E. Bouma, Quantitative depolarization measurements for fiber-based polarization-sensitive optical frequency domain imaging of the retinal pigment epithelium. Journal of Biophotonics, 2019. 12(1): p. e201800156.

27. Christopher P Favazza, O.J., Lynn A Cornelius, Lihong V Wang, In vivo photoacoustic microscopy of human cutaneous microvasculature and a nevus. Journal of Biomedical Optics, 2011. 16(1): p. 016015.
28. Xiao Shu, H.L., Biqin Dong, Cheng Sun, and Hao F. Zhang, Quantifying melanin concentration in retinal pigment epithelium using broadband photoacoustic microscopy. Biomedical Optics Express, 2017. 8(6): p. 2851-2865.
29. Zhiyang Wang, Y.C., Shu Pan, Wuyu Zhang, Ziwei Guo, Yuzhi Wang, Sihua Yang, Quantitative classification of melasma with photoacoustic microscopy: a pilot study. Journal of Biomedical Optics, 2024. 29: p. S11504.
30. Koji Mizukoshi, H.I., Taiichiro Ida, Quantitative analysis of age-related changes in vascular structure, oxygen saturation, and epidermal melanin structure using photoacoustic methods. Skin Res Technol., 2024. 30: p. e13537.
31. Yasuyuki Tsunoi, N.S., Izumi Nishidate, Fumiyuki Ichihashi, Daizoh Saitoh, Shunichi Sato, Burn depth assessment by dual-wavelength light emitting diodes-excited photoacoustic imaging in rats. Wound Repair and Regeneration, 2022. 31(1): p. 69-76.
32. Razansky, S.M.a.D., Photoacoustics: a historical review. Advances in Optics and Photonics, 2016. 8(4): p. 586-617.
33. Jokerst, Y.M.a.J.V., Engineering Plasmonic Nanoparticles for Enhanced Photoacoustic Imaging. ACS Nano, 2020. 14(8): p. 9408-9422.
34. Ali Afshari, R.B.S., David Burgos, William C Vogt, Jianting Wang, Gonzalo Mendoza, Sandy Weininger, Kung-Bin Sung, Anthony J Durkin, T Joshua Pfefer, Evaluation of the robustness of cerebral oximetry to variations in skin pigmentation using a tissue-simulating phantom. Biomedical Optics Express, 2022. 13(5): p. 2909-2928.
35. Igor V Meglinski, S.J.M., Quantitative assessment of skin layers absorption and skin reflectance spectra simulation in the visible and near-infrared spectral regions. Physiol. Meas., 2002. 23(4): p. 741-753.
36. Jacques, S.L., Optical properties of biological tissues: A review. Physics in Medicine & Biology, 2013. 58: p. R37-61.
37. Ronneberger, O., P. Fischer, and T. Brox, U-Net: Convolutional Networks for Biomedical Image Segmentation. Int. Conf. Medical Image Computing and Computer-Assisted Intervention (MICCAI), 2015: p. 234–241.
38. Kong, C., et al., Automatic algorithm for the characterization of sweat ducts in a three-dimensional fingerprint. Optics Express, 2021. 29(19): p. 30706-30714.
39. Enrico Dimitrow, M.Z., Martin Johannes Koehler, Johannes Norgauer, Karsten König, Peter Elsner, Martin Kaatz, Sensitivity and specificity of multiphoton laser tomography for in vivo and ex vivo diagnosis of malignant melanoma. Journal of Inverstigative Dermatolog, 2009. 129(7): p. 1752-1758.
40. Ilse Hurbain, M.R., Peggy Sextius, Emilie Bourreau, Céline Marchal, Françoise Bernerd, Christine Duval, Graça Raposo, Melanosome Distribution in Keratinocytes in Different Skin Types: Melanosome Clusters Are Not Degradative Organelles. Journal of Inverstigative Dermatolog, 2018. 138(3): p. 647-656.
41. Aditya K. Gupta, M.D.G., Keyvan Nouri, Susan Taylor, The treatment of melasma: A review of clinical trials. Journal of the American Academy of Dermatology, 2006. 55(6): p. 1048-1065.